A&A 400, 319–328 (2003)
DOI: 10.1051/0004-6361:20021862

Astronomy & Astrophysics

On the shock-induced variability of emission lines in M-type Mira variables

II. Fe II and [Fe II] emission lines as a diagnostic tool

He. Richter[1], P. R. Wood[2], P. Woitke[1], U. Bolick[1], and E. Sedlmayr[1]

[1] Zentrum für Astronomie und Astrophysik, TU Berlin, Sekr. PN 8-1, Hardenbergstraße 36, 10623 Berlin, Germany
[2] Research School of Astronomy and Astrophysics, Australian National University, Cotter Road, Weston ACT 2611, Australia
e-mail: wood@mso.anu.edu.au

Received 29 July 2002 / Accepted 16 December 2002

Abstract. Our observations of cool, shock penetrated, expanding atmospheres of M-type Mira variables (Richter & Wood 2001) have suggested that the emission lines of Fe II and [Fe II] can serve as an excellent diagnostic tool to study the hydro- and thermodynamical conditions in the shocked regions close to the photosphere of these stars. Here we present a series of detailed NLTE (Non Local Thermodynamic Equilibrium) radiative transfer calculations, which have been performed on structures resulting from thermodynamical models of periodic shock waves, in order to calculate the emergent Fe II and [Fe II] emission line fluxes and to analyse the conditions which lead to their formation. Our basic parameter studies reveal that the ionised iron lines originate from the hot post-shock zone and that they are in fact emitted close to the star's photosphere. Furthermore, the modelling of the Fe II and [Fe II] emission line fluxes determine a specified limit of the shock velocity amplitude and pre-shock density for the innermost shocks. This offers an unique possibility to determine the thermodynamical conditions in the inner dust formation zone and thereby will shed some light on the basic mechanism of dust formation in M-type Mira stars.

Key words. line: formation – shock waves – radiative transfer – stars: late-type – stars: variables: general

1. Introduction

The high mass loss rate of Miras of the order of $10^{-6}\,M_{\odot}\,\mathrm{yr}^{-1}$ (Habing 1996) are probably generated by a combination of pulsation of the star and radiation pressure on newly formed dust grains (Wood 1979; Bowen 1988; Fleischer et al. 1992; Feuchtinger et al. 1993; Höfner & Dorfi 1997; Winters et al. 2000). Pulsation generates shock waves which propagate through the atmosphere, thereby increasing the mass density in the outer parts of the atmosphere. The passage of a shock leads to a sudden increase of the pressure, density and temperature of the gas. Behind the shock, the gas cools via the emission of radiation, which leads to conditions that are favourable for dust formation. The shocks in the outer parts of the atmosphere thereby trigger dust formation. Radiation pressure on these dust grains finally drives the wind of these stars with high mass loss rates.

Although dust plays a central role in driving mass loss in the hydrodynamical models, the details of the dust formation process as caused by shock waves is still not fully understood. Also it is still not proved whether the predictions of the hydrodynamical models are consistent with the reality of Mira stars. A combination of detailed observation and theory is required to test the hydrodynamical models.

The hydrodynamical conditions of the dust-forming layers of the atmosphere can be studied by metal emission lines, which appear late in the pulsation cycle of M-type Mira variables when the shock wave has reached these layers. In particular the Fe II and [Fe II] emission lines can serve as an excellent diagnostic tool to study these according layers. The erratic appearance of these particular emission lines only in stars which have just had a bright light maximum suggests that they require an exceptionally bright maximum for excitation (Richter & Wood 2001). Presumably, the bright maxima are associated with stronger shock waves caused by the stellar pulsation.

In order to model the Fe II and [Fe II] emission lines and to analyse the hydro- and thermodynamical conditions which lead to their formation, we carried out basic parameter studies with detailed NLTE radiative transfer calculations (Sect. 2) performed on a series of radial shock structures (Sect. 3). In combination with constraints on these lines derived from our observations (Sect. 4), we found limited ranges of pre-shock density ρ_{pre}, shock velocity amplitude Δv and radial distance from the centre of the star of the shock R for which fitting of the Fe II and [Fe II] line fluxes to observations was successful (Sects. 5.1 and 5.2).

Send offprint requests to: He. Richter,
e-mail: richter@astro.physik.tu-berlin.de

2. NLTE radiative transfer

In order to handle the shocked atmospheres of Mira variable, the NLTE radiative line transfer is calculated on *snapshots* of hydrodynamical shock wave structures (time-independent radiative transfer). Let us give a brief explanation why this method is appropriate: In *LTE* the diffusion time for photons at large optical depth $t_{\rm diff} = l/c$ is much smaller than the hydrodynamical time scale $t_{\rm hydro} = L/a$, because $L \gg l$ and $a \ll c$ (L: scale hight of the atmosphere, l: mean free path of photons, a: sound speed and c: speed of light). *Here the assumption of a snapshot is well justified*. However for *NLTE* this situation changes: the thermalisation parameter ϵ (roughly the ratio of collision rates to spontaneous emission rates) enters the consideration and then $t_{\rm diff}/t_{\rm hydro} \sim \frac{(la)/(Lc)}{\epsilon^2}$. The thermalisation parameter becomes much smaller than 1 in regions of line formation, hence $t_{\rm diff}/t_{\rm hydro} \gg 1$, so a snapshot would *not* be justified. However, the extreme velocity gradient in the shock sets an upper limit to the optical depth a photon must penetrate before it can escape freely. For shocks the interaction region becomes very small and hence the radiation is only coupled to the local conditions again. *The assumption of snapshot is therewith justified in this case, too* (private communication with D. Mihalas).

The geometry chosen in our code is spherically symmetric, which has the advantage of achieving a general tool to study regions close to the photosphere (∼planar), but also the extended circumstellar envelopes of Mira variables.

Our code accounts for arbitrary velocity fields by using the comoving frame formalism (Mihalas et al. 1975), which is essential if one studies shock waves.

With all the named assumptions we obtain the following form of the radiative transfer equation:

$$\mu\frac{\partial I_\nu}{\partial r} + \frac{1-\mu^2}{r}\frac{\partial I_\nu}{\partial \mu} - \frac{\nu_0\, v(r)}{c\, r}\left(\mu^2\frac{{\rm d}\ln v(r)}{{\rm d}\ln r} + 1 - \mu^2\right)\frac{\partial I_\nu}{\partial \nu} = \eta_\nu - \chi_\nu I_\nu \ , \tag{1}$$

with $\mu = \cos\theta$, I_ν: frequency and spatial dependent intensity, ν_0: laboratory frequency of the line centre, $v(r)$: velocity field, η_ν: frequency dependent emissivity and χ_ν: frequency dependent absorption, which are given by:

$$\begin{aligned}\eta_\nu &= \eta_{\rm l}\,\phi_\nu + \eta_{\rm c} + \eta_{\rm sca},\\ \chi_\nu &= \chi_{\rm l}\,\phi_\nu + \chi_{\rm c} + \chi_{\rm sca}\end{aligned} \tag{2}$$

(indices l: line, c: continuum and sca: scattering).

We assume complete redistribution, hence, the profile function for absorption and emission are given by the same Voigt profile ϕ_ν in our calculations. For our investigations of regions close to the star's photosphere, Thompson scattering by electrons is considered to be the main contribution to the scattering term. The continuum is described by a constant opacity $\chi_{\rm c}(r) = 2\times10^{-4}\rho(r)$ following the radial density structure of the gas $\rho(r)$ according to Bowen (1988). The line opacities for NLTE are given, if the occupation numbers of all atomic levels are known, hence, the radiative transfer equation is coupled with the rate equation system. The occupation numbers of each level i considering all atomic levels j are calculated by solving the corresponding rate equation

$$\sum_{j>i} n_j(A_{ji} + B_{ji}\overline{J}) + \sum_{j<i} n_j B_{ji}\overline{J} + \sum_{j\neq i} n_j C_{ji} = \sum_{j>i} n_i B_{ij}\overline{J} + \sum_{j<i} n_i(A_{ij} + B_{ij}\overline{J}) + \sum_{j\neq i} n_i C_{ij}, \tag{3}$$

where n is the occupation number of the level, A and B are the Einstein coefficients for spontaneous emission, induced emission and absorption, C the collision rates of the corresponding transitions and $\overline{J}$ the mean, frequency integrated intensity. The left hand side of Eq. (3) represents the gain terms for level i whereas the right hand side represents the loss terms.

To solve this system we use a Gauss-solver for the rate equation and an adjusted, damped newton iteration. As a numerical approach to handle the NLTE radiative transfer equation (Eq. (1)) we utilised the Feautrier method, where the equations are treated with a 2nd order (partly 1st) discretisation according to Richtmyer & Morton (1967). Additionally, one needs an iteration to solve this equation, which is necessary because of the consideration of scattering, by which the radiative transfer equation becomes an integro-differential equation. For our studies we are using the accelerated lambda operator (ALO) (Puls 1991; Rybicki & Hummer 1991). This yields a stable numerical solution of the radiative transfer in our experience.

The input data that our NLTE radiative transfer code requires is a radial thermodynamical structure consisting of the velocity of the gas $v(r)$, gas density $\rho(r)$, gas temperature $T_{\rm g}(r)$ and the Fe II and electron densities $n_{\rm FeII}$, $n_{\rm el}$. For this application we compute detailed shock structures in Mira variable stars in regions close to the photosphere at $\sim$1−6 R_* (Sect. 3).

With regard to our observations, the regions close to the star's photosphere are of particular interest for the formation of Fe II and [Fe II] emission lines. To investigate these lines, the FeII-model-atom is so far treated as a 3-level-atom, including one permitted line: M38, 4583.84 Å and one forbidden emission line: 6F, 4417.51 Å (data taken from the CHIANTI database[1]; Dere et al. 1997). This case represents a model-atom which is easy to handle and where individual rates and level population numbers can be checked straightforwardly. These preliminary calculations already give some first insights into the formation of the permitted and forbidden Fe II lines (it is planned to enlarge the model-atom towards a more realistic 142-level atom in the near future).

The code has so far been utilised to model various rotational-vibrational CO absorption lines in the cool circumstellar envelopes of Long Period Variables (Bolick et al. 2003), where the NLTE radiative line transfer has been calculated for complete envelopes extending to ∼1000 R_*.

3. Radial shock structures

The radial shock structures used as input models were obtained from detailed thermodynamical models in which the gas elements are assumed to move on ballistic trajectories (Woitke et al. 1996b): we call these "gas-box" models. For each

[1] http://wwwsolar.nrl.navy.mil/chianti.html

Lagrangian mass element, we solve the first law of thermodynamics in the form

$$\frac{\mathrm{d}h}{\mathrm{d}t} = V\frac{\mathrm{d}p}{\mathrm{d}t} + Q_{\rm rad}. \quad (4)$$

$h = e + pV$ is the specific enthalpy of the gas, $V = 1/\rho$ the specific volume, p the gas pressure and $Q_{\rm rad}$ the net radiative heating function. At each full period $t = nP$ (P is the pulsation period of the star), the classical Rankine Hugoniot relations are solved in order to determine the post-shock state (h_2, p_2, v_2) from the pre-shock state (h_1, p_1, v_1). v_1 is the given shock velocity and v_2 the velocity of the post-shock gas in a reference frame comoving with the shock front. During each period, $p(t)$ is a prescribed function (see Eq. (1) in Woitke et al. 1996b), varying continuously from $p\,(t{=}nP) = p_2$ back to $p\,(t{=}nP{+}P{-}\epsilon) = p_1$. The calculations were repeated with p_1, v_1 fixed until all thermodynamical variations have become periodical.

The resulting time-variations of all quantities in the Lagrangian mass element depend strongly on the treatment of the state functions and, in particular, on the radiative heating/cooling rate $Q_{\rm rad}$. We have developed a detailed NLTE gas model in which all particle densities (neutral atoms, molecules, electrons and single ions) and level populations are calculated in statistical equilibrium under the influence of a continuous background radiation field $J_\nu^{\rm cont}$ (Woitke et al. 1996a). The gas is assumed to be optically thin in the continuum, whereas optical depth effects in spectral lines are accounted for by applying Sobolev theory according to the local mean velocity gradient $\langle \mathrm{d}v/\mathrm{d}l\rangle$. The net radiative heating function $Q_{\rm rad}$, defined as the net photon energy exchange rate between radiation field and matter, is determined from the various free-free and bound-free (b-f) transitions, atomic lines and molecular ro-vibrational transitions. The model atoms include several thousand permitted and forbidden lines, and b-f transitions from excited levels (Woitke & Sedlmayr 1999). In addition to the photo-ionisation and direct recombination rates, collisional ionisation from all neutral (ground and excited) levels are included, which affects i.e. the determination of the electron and the Fe II particle densities.

In this application, we assume a continuous black-body background radiation field $J_\nu^{\rm cont} = B_\nu(T_{\rm rad})$. The radiation temperature $T_{\rm rad}$ is assumed to be related to the distance by

$$T_{\rm rad}^4 = \frac{1}{2}T_*^4\Big(1 - \sqrt{1 - R_*^2/R^2}\Big), \quad (5)$$

where T_*, R_* and R are the stellar temperature, the stellar radius and the considered radial distance of the shock front, respectively. In the special case of a undiluted Planck field, radiative equilibrium ($Q_{\rm rad} = 0$) is established if and only if $T_{\rm g} = T_{\rm rad}$. Concerning the mean velocity gradient, a fixed value of $\langle \mathrm{d}v/\mathrm{d}l\rangle = 10^{-7}\ \mathrm{s}^{-1}$ is used, a typical value for the saw-tooth like velocity fields encountered in the shocked envelopes of Mira stars.

Finally, the radial structure of the shock wave in the Eulerian frame (denoted by $'$) can be approximately reconstructed from the calculated thermodynamic variations in the Lagrangian element by assuming ballistic trajectories with position $r'_{\rm M}(t) = r'_{\rm M}(0){+}a\,t{-}b\,t^2$ as sketched in Fig. 1. The velocity

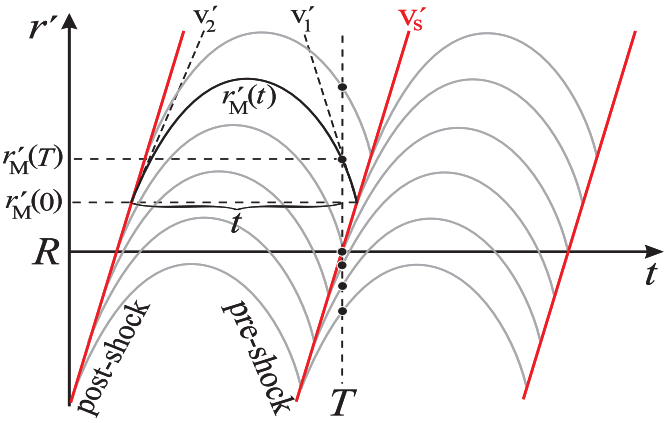

Fig. 1. Reconstruction of the radial structure of a shock wave at position R for time T (dots) from periodically shocked Lagrangian elements assuming ballistic trajectories (grey lines). Dark grey lines indicate the trajectories of the periodic shock fronts.

amplitude of the shock wave is introduced as $\Delta v = v'_2 - v'_1 = v_1 - v_2 = v_1(1{-}\rho_1/\rho_2)$. We assume that the velocity of the shock front in the Eulerian frame $v'_{\rm s} = \frac{\Delta v}{2}\frac{\rho_2+\rho_1}{\rho_2-\rho_1}$ is constant and that all mass elements undergo the same periodical variations, thereby neglecting the general trend of decreasing pre-shock densities and background radiation fields in the considered (small) radius interval.

From the condition of periodicity, the given value of Δv and the requirement that $r'_{\rm M}(0)$ must be located on one of the shock wave trajectories, the quantities a, b and $r'_{\rm M}(0)$ can be determined. The resulting radial position $r'_{\rm M}(T)$ and velocity $v'_{\rm M}(T)$ of the Lagrangian mass element at the snapshot-time T are

$$r'_{\rm M}(T) = \begin{cases} R - v'_{\rm s}(t-P) + v'_2\,t\left(1-\frac{t}{P}\right), & t > \frac{P}{2} \\ R - v'_{\rm s}t + v'_2\,t\left(1-\frac{t}{P}\right), & t \le \frac{P}{2} \end{cases} \quad (6)$$

$$v'_{\rm M}(T) = v'_2 + (v'_1 - v'_2)\,\frac{t}{P}. \quad (7)$$

All other quantities of interest at the point $r'_{\rm M}(T)$, here $T_{\rm g}(t)$, $n_{\rm el}(t)$ and $n_{\rm Fe\,II}(t)$, are taken from the Lagrangian gas-box model at time t, which is the time since the last shock wave encounter.

4. Observational constraints

Our observations (Richter & Wood 2001) showed that the permitted Fe II line of the multiplet M 38 (4583.84 Å) and the forbidden line [Fe II] 6F (4417.51 Å) – among other forbidden lines [Fe II] 7F, and [Fe II] 21F – belong to the faintest emission lines observed. The Fe II and [Fe II] lines were observed at late phases around minimum visible light $\phi \sim 0.3{-}0.5$ in stars which have just had a bright light maximum. The emission line profiles of the M 38 and 6F lines are roughly Gauss-like in our observations with no systematic line shifts, i.e. velocity difference, and both lines were always detected simultaneously.

To estimate the region of emission we assume a pulsation period of 1 yr and a shock wave velocity in the Eulerian frame[2]

[2] Note that the observed shock velocity $v_{\rm obs}$ is to be identified with the sum of the velocity of the hot post-shock gas (v'_2 in Sect. 3) and the underlying mean wind velocity.

of $v_s' = 10-40\,\mathrm{km\,s^{-1}}$ which leads to a distance of $1-4\,R_*$ that the shock front travels in one period. With the assumption that the shock emerges from the photosphere (defined to be at optical depth one) at maximum $\phi = 0.0$, the radial position of the shock front R around minimum ($\phi = 0.5$) can be approximated as $\sim R = 1.5-3\,R_*$. (This rough approximation neglects the shock deceleration on the way through the atmosphere and the underlying wind velocity profile.) In summary one can conclude from the observations:

- The Fe II (M 38) and [Fe II] 6F emission lines show up simultaneously.
- Both lines have Gauss-like profiles with no systematic difference in velocity.
- Normalised peak fluxes $F_\mathrm{n} = F_\mathrm{line}^\mathrm{peak}/F_\mathrm{cont}$ are in the limits $1.2 < F_\mathrm{n} < 10$ (lower limit is detection limit).
- The line ratios are $F_\mathrm{M38}/F_\mathrm{6F} \sim 1$.
- The lines should originate from a region $\sim$1.5–3 R_*.

5. Fe II and Fe II line fluxes

Our complete procedure for computing Fe II and [Fe II] line fluxes is: (1) choose values for the radius R of the shock front, the shock velocity amplitude Δv and the pre-shock density ρ_pre; (2) iterate the gas-box model to a periodic solution in order to get the thermodynamic properties of the gas (T, ρ, ionisation state, etc.) as a function of radius (or, equivalently, distance behind the shock front); and (3) use the thermodynamic properties from the gas-box model in the NLTE radiative transfer code in order to get the line fluxes and profiles.

In order to try to reproduce the observed normalised peak fluxes of the ionised iron lines, a wide range of models have been constructed. One can in principle vary the 3 parameters in the gas-box calculations: the radial position of the shock front R, the shock velocity amplitude Δv and the pre-shock density ρ_pre ($\equiv\rho_1$ in Sect. 3). We carried out two different parameter studies, namely a variation of ρ_pre in a series of models where Δv is specified as a function of R (Sect. 5.1), and a variation of Δv in a series of models where ρ_pre is specified as a function of R (Sect. 5.2).

The approximated relations between R and Δv as well as R and ρ_pre were derived from a reference model by Schirrmacher et al. (2002), which is a detailed hydrodynamical calculation of a C Mira variable based on the CHILD-code (Fleischer et al. 1992) with included NLTE heating- and cooling functions (Woitke et al. 1996a). The model has period $P = 310$ d, stellar mass $M_* = 1\,M_\odot$, effective temperature $T_\mathrm{eff} = 3000$ K and luminosity $L_* = 4760\,L_\odot$, carbon to oxygen ration C/O = 1.8 and piston amplitude $\triangle u = 2\,\mathrm{km\,s^{-1}}$. Apart from the C/O-ratio, these parameters should be appropriate for the M-type Mira stars studied by Richter & Wood (2001). Note that presently the only self-consistent hydrodynamical models available for oxygen-rich Miras are the ones of Jeong (2000), which unfortunately do not result in high temperature peaks up to $\sim 10^4$ K in the inner $1-5\,R_*$ because no NLTE heating- and cooling functions are yet included. We had to compromise by taking a carbon-rich model as a reference, which nevertheless gives a good idea of the parameter range of ρ_pre and Δv in a Mira atmosphere. We stress that our gas-box calculations were carried out with an oxygen-rich composition. The radial structures from these gas-box calculations were used as input models for the detailed NLTE radiative line transfer calculations – the reference model was only used to guide our choice of input parameters for the gas-box models.

Our radiative transfer code requires a complete radial thermodynamical structure as input. For cases where the shock was far out in the atmosphere, all inner grid points from $1\,R_*$ up to the last given innermost grid point of the gas-box model were assumed to have the thermodynamical conditions at this innermost grid point. Examination of these models shows that the innermost regions, which are far down stream from the thin, ionised post-shock zones, do not contribute to the Fe II line fluxes anyway so this procedure should not lead to significant errors.

The normalised peak fluxes $F_\mathrm{n} = F_\mathrm{line}^\mathrm{peak}/F_\mathrm{cont}$ resulting from each model are sorted into three categories: those within the observed limit $1.2 < F_\mathrm{n} < 10$, those smaller than the detection limit $F_\mathrm{n} < 1.2$ and those bigger than the observed limit $F_\mathrm{n} > 10$. Black lines, light grey lines and dark grey lines, respectively, are used to indicated the regions of parameter space where models belonging to these categories lie in Figs. 2, 3 and 6.

5.1. Variation of ρ_{pre}

For a variety of fixed pairs of R and Δv the pre-shock density ρ_pre was varied, resulting in about 750 gas-box models. Figure 2 depicts a parameter study up to 5 R_* with intermediate shock amplitudes (additional parameter studies for 5–10 R_* with $\Delta v < 18\,\mathrm{km\,s^{-1}}$ gave normalised peak fluxes which were too small so they are not depicted here). Also marked with a dotted-dashed line in Fig. 2 is a relation between pre-shock density and shock position, which was derived from the model by Schirrmacher et al. (2002), to give a reference for the expected parameter range of ρ_pre in a Mira atmosphere.

Note, that we are not prescribing that shocks *do* have the velocities we modelled here. We are just testing parameter space to see what parameters explain the observations. In that respect, not all parameter combinations near the dotted-dashed line in Fig. 2 have to be realised in Mira atmospheres, because the shock velocity amplitudes at a given radius can be quite different than chosen for this study (see also Sect. 5.1.2). However, the observational finding that FeII and [FeII] emission fade away shortly after minimum light suggests that the shock velocity amplitude in fact decreases quickly to values that are too low to produce emission.

5.1.1. Outstanding regions in the ρ_pre, R space

The normalised line fluxes of the forbidden and the permitted line are both within the observed limits close to the star $R = 1-2.5\,R_*$ (Fig. 2, black lines), then around $R = 3\,R_*$ both normalised line fluxes turn out to be too large (Fig. 2, grey lines) whereas they are much too small in the regions $R = 3.5-5\,R_*$ (Fig. 2, light grey lines). This is mainly due to the

decrease of Δv in our models (see also Sect. 5.1.3). Generally, for models with $\rho_{\rm pre} > 10^{-14}$ g cm^{-3} the normalised peak fluxes of the FeII-lines turn out to be too large (Fig. 2, dark grey lines). These pre-shock densities are larger than the derived radial pre-shock densities resulting from the reference model.

Two especially outstanding domains can be seen in Fig. 2:

• **Region A:** A remarkable result presented in Fig. 2 is that there exists *only one domain*, namely region A, where the normalised peak flux of both calculated permitted and forbidden lines fit the observed fluxes. This region is close to the star's photosphere at $R = 1.2{-}1.8\,R_*$ and the densities therein correspond to our reference model in the upper limit, respectively being one order of magnitude smaller for the lower limit of region A. Additionally, region A fits the approximated position of the shock-front R around phase $\phi \sim 0.3$–0.5 (see also Sect. 4).

• **Region B:** In this region at about $R = 3.5{-}4.5\,R_*$ the forbidden line fits the observed limits, but the permitted line is below the detection limit. As both lines were always observed simultaneously, this finding does not correspond to our observations. The pre-shock density in region B is too high according to our reference model (∼1.5–3 orders of magnitude higher). In addition, these lines could only be emitted from a shock ∼1.5 cycles old (i.e. from the previous pulsation cycle) since even an extreme shock with velocity $v_{\rm s}' = 40$ km s^{-1} could at most reach $R = 3\,R_*$ around phase $\phi = 0.5$. However a shock with $v_{\rm s}' = 10$ km s^{-1} could reach $R = 3.5\,R_*$ at $\phi = 1.5$.

Further examination shows that all gas-box models in region A have Fe II ion densities of $n_{\rm FeII} \sim 10^5{-}10^{5.5}$ cm^{-3} in the hot post-shock region. Higher (lower) ion densities generate normalised peak fluxes that are too large (small). We found that the Fe II density is the most important factor determinining the calculated normalised peak fluxes. These results lead to the conclusion that the Fe II emission lines can only originate from the hot post-shock region, where $n_{\rm FeII} \sim 10^5{-}10^{5.5}$ cm^{-3}. The cooler post-shock regions do not contribute to the calculated fluxes.

5.1.2. The effect of Δv on region A

We have additionaly investigated the influence of different shock velocity amplitudes in the models in order to study how the position of region A changes. We assumed the same pre-shock densities as before and calculated models with varied velocity amplitudes of the shock wave in the interval $1{-}2.1\,R_*$ (about 200 models for each study).

Our investigations show that *higher* shock velocity amplitudes shift region A towards *lower* pre-shock densities (left panel in Fig. 3) and *lower* velocities cause a shift towards *higher* densities (right panel in Fig. 3). It can also be noted, that the details of the shape of region A are slightly changed: For lower shock velocity amplitudes the region is located around $\rho_{\rm pre} \sim 10^{-14}$ g cm^{-3}, whereas it is more spread out for higher shock velocity amplitudes from $\rho_{\rm pre} \sim 10^{-14.5}$ g cm^{-3} to $10^{-16.5}$ g cm^{-3}. Generaly, *no shift* in the radial distance of region A results.

As with our earlier set of models with varying $\rho_{\rm pre}$, a detailed examination of our models shows that an ion density in the gas-box models of about $n_{\rm FeII} \sim 10^5{-}10^{5.5}$ cm^{-3} is required in models that reproduce the observed forbidden and permitted line fluxes.

5.1.3. Sample models

Several models marked around region A in Fig. 2 are depicted in Fig. 4. These models cover the full range of observed fluxes. As noted above, we found that $n_{\rm FeII}$ is the limiting factor for the line fluxes, so in the following we want to outline the factors that influence the particle density of Fe II.

The upper panels of Fig. 4 show the corresponding gas-box models for a $\Delta v = 30$ km s^{-1} shock wave at $R = 1.5\,R_*$ approaching pre-shock densities of 5×10^{-16}, 2×10^{-15} and 6×10^{-15} g cm^{-3}. According to the model, the Fe II densities clearly follow the temporal evolution of the temperature. This strong correlation demonstrates the importance of the collisional ionisation processes (note, however, that we have not considered the photo-ionisation of Fe in any "radiative precursor" due to UV radiation emergent from the shock wave itself, see e.g. Huguet et al. 1992). In our shock model, the formation of Fe II lines is clearly restricted to the high-temperature regions behind the shock waves.

The post-shock ("peak") temperature is determined from the amount of mechanical energy dissipated by the shock wave and the pre-shock state, utilising the Rankine-Hugoniot relations and the assumption of statistical equilibrium. If the pre-shock gas is H_2-rich, only shock waves with velocities $\gtrsim 20$ km s^{-1} are able to completely dissociate the H_2 molecules. The surplus mechanical energy is converted into thermal kinetic energy, leading easily to post shock temperatures of the order of $\approx 8000...11000$ K. At these temperatures, the H atoms are ionised (mainly collisionally) which again consumes a lot of the dissipated energy. Behind the shock front, the gas cools via radiative cooling in two phases. First mainly the hydrogen b-f transitions, Lyα and Hα as well as Ca II H + K and Mg II h + k lead to a quick temperature decrease down to about 5000–6000 K within a very narrow region behind the shock (not resolved in Fig. 4). Then permitted lines can no longer be excited collisionally and low-lying energy levels of certain forbidden and fine-structure lines, in particular of Fe I and Fe II, take over and the radiative cooling slowly continues (Woitke & Sedlmayr 1999) until temperatures appropriate for molecule formation are reached. Once the first molecules are present in the gas phase, the large amount of permitted rovibrational lines of polar molecules, in particular CO, causes a substantial re-increase of the radiative cooling rate and finally results in a fast relaxation towards radiative equilibrium.

The radial extent of the complete radiative post-shock zone amounts to $\sim 0.035\,R_*$, $\sim 0.01\,R_*$ and $\sim 0.005\,R_*$ for pre-shock densities 5×10^{-16} g cm^{-3} (H85), 2×10^{-15} g cm^{-3} (H91) and 6×10^{-15} g cm^{-3} (H95), respectively – a consequence of the general trend of increasing radiative cooling rates per unit mass with increasing densities.

In summary, Fe II emission lines are expected to occur if the velocity is $\gtrsim 20$ km s^{-1} ("dissociative shock") or if the pre-shock state is H_2-poor.

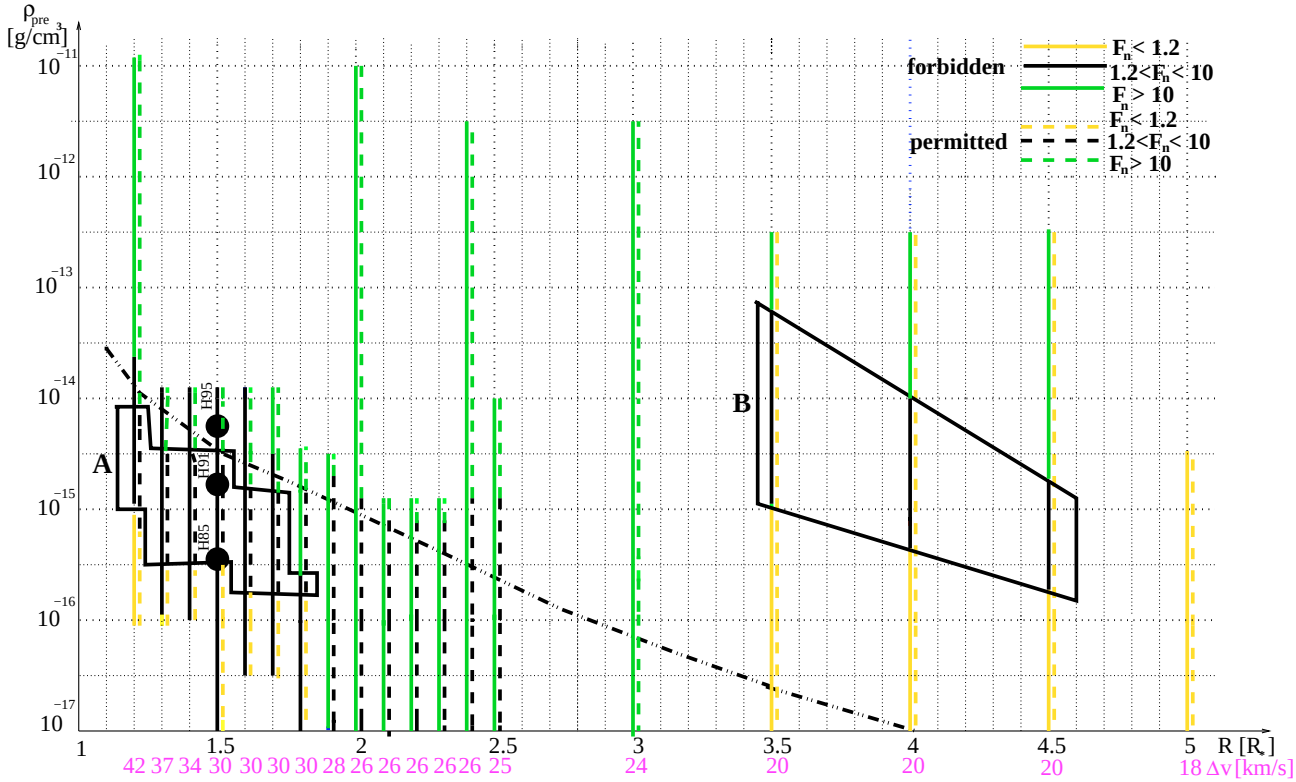

Fig. 2. Parameter study for the normalised peak line fluxes of the forbidden transition [Fe II] 6F (solid lines) and permitted transition Fe II M38 (dashed lines). Models were constructed with a range of $\rho_{\rm pre}$ for each chosen radius R and Δv pair: the radius R and Δv pairs are marked on the x-axis. Black lines mark ranges of $\rho_{\rm pre}$ where the calculated normalised peak fluxes are within the observational limit, light grey lines mark ranges where the fluxes are lower than observed, and dark grey lines mark ranges where the fluxes are larger than the observed limit. A radial pre-shock density structure from a hydrodynamical model of Schirrmacher et al. (2002) is depicted by the dotted-dashed line. Region A (bounded by a solid black line) delineates the area where both permitted and forbidden line fluxes are consistent with observations, while in region B the forbidden line fluxes agree with observed values but the permitted line fluxes do not. Bullets mark models shown in Fig. 4.

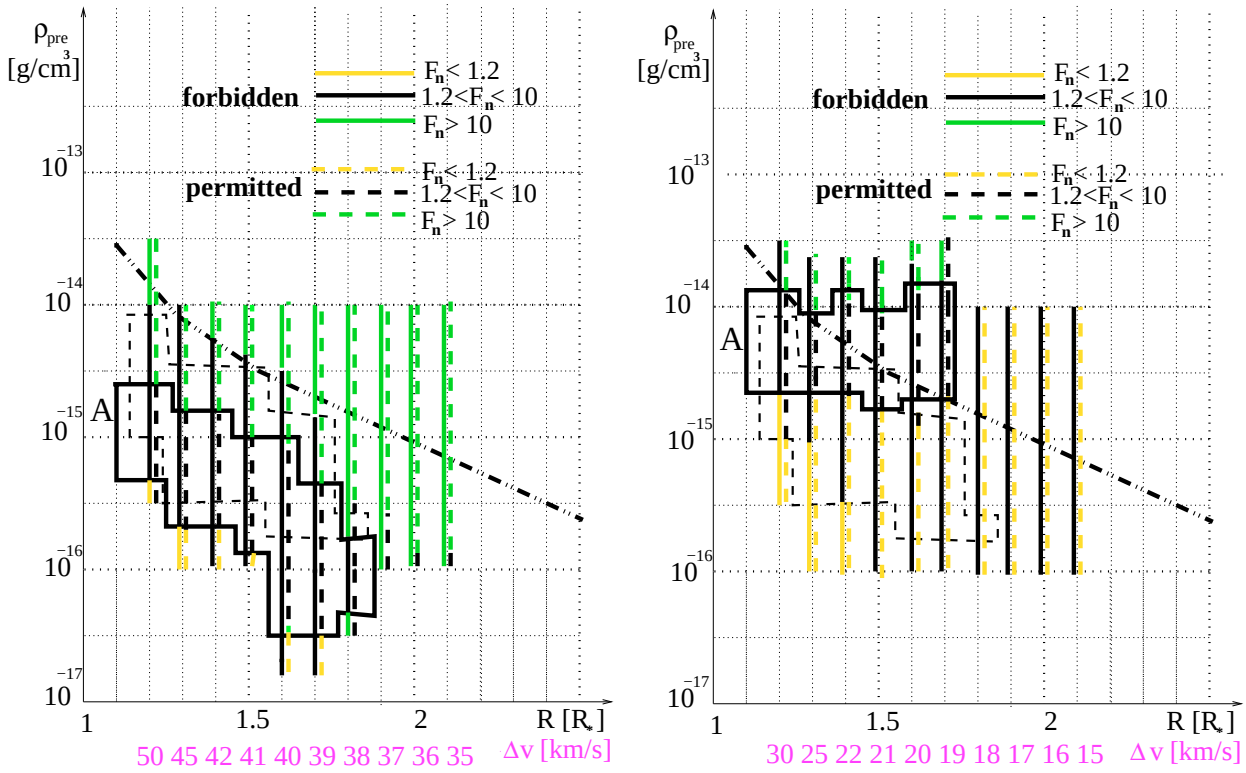

Fig. 3. Same as Fig. 2 but for Δv higher (left) or lower (right) at a given radius than in Fig. 2.

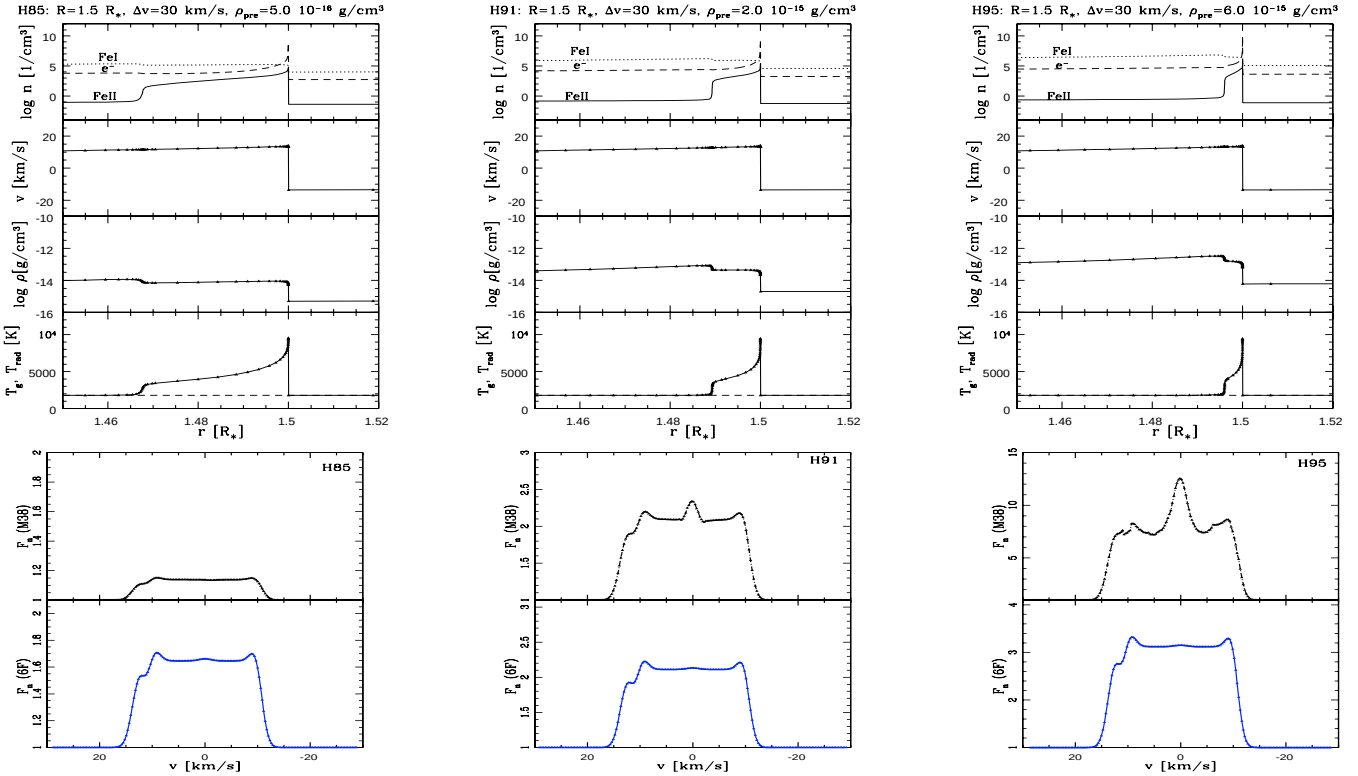

Fig. 4. Three models from region A (bullets in Fig. 2) ordered from left to right by increasing pre-shock density. *Upper row:* gas-box shock models: particle densities $n(r)$ of Fe II, Fe I and electrons; radial velocity $v(r)$; density $\rho(r)$; gas temperature $T_{\rm g}(r)$ and radiation temperature $T_{\rm rad}(r)$ (dashed). *Lower row:* resulting NLTE line fluxes in units of normalised flux $F_{\rm n}$: permitted M38 transition (upper panels), forbidden 6F transition (lower panels).

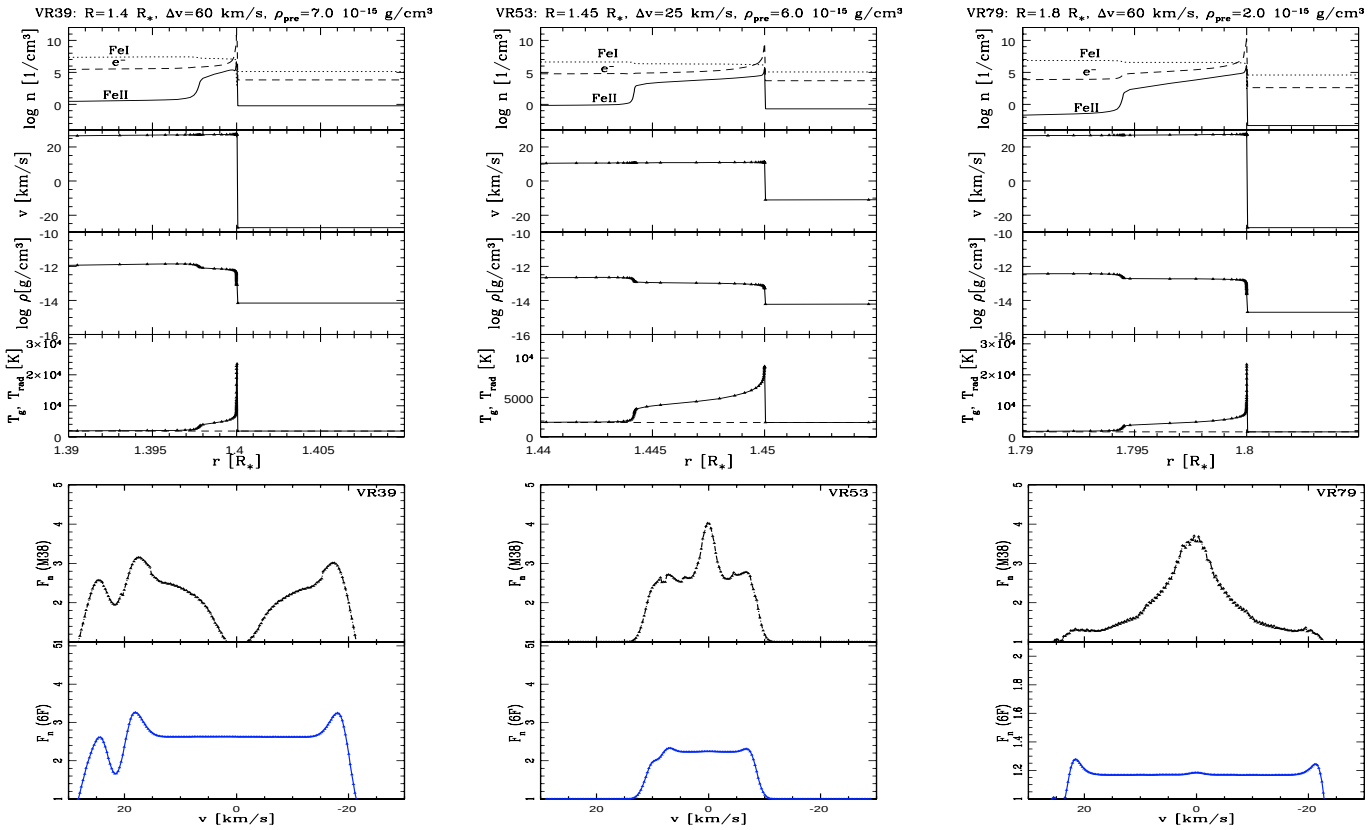

Fig. 5. Same as Fig. 4 but for models from regions B3, A1 and A2 in Fig. 6 (from left to right).

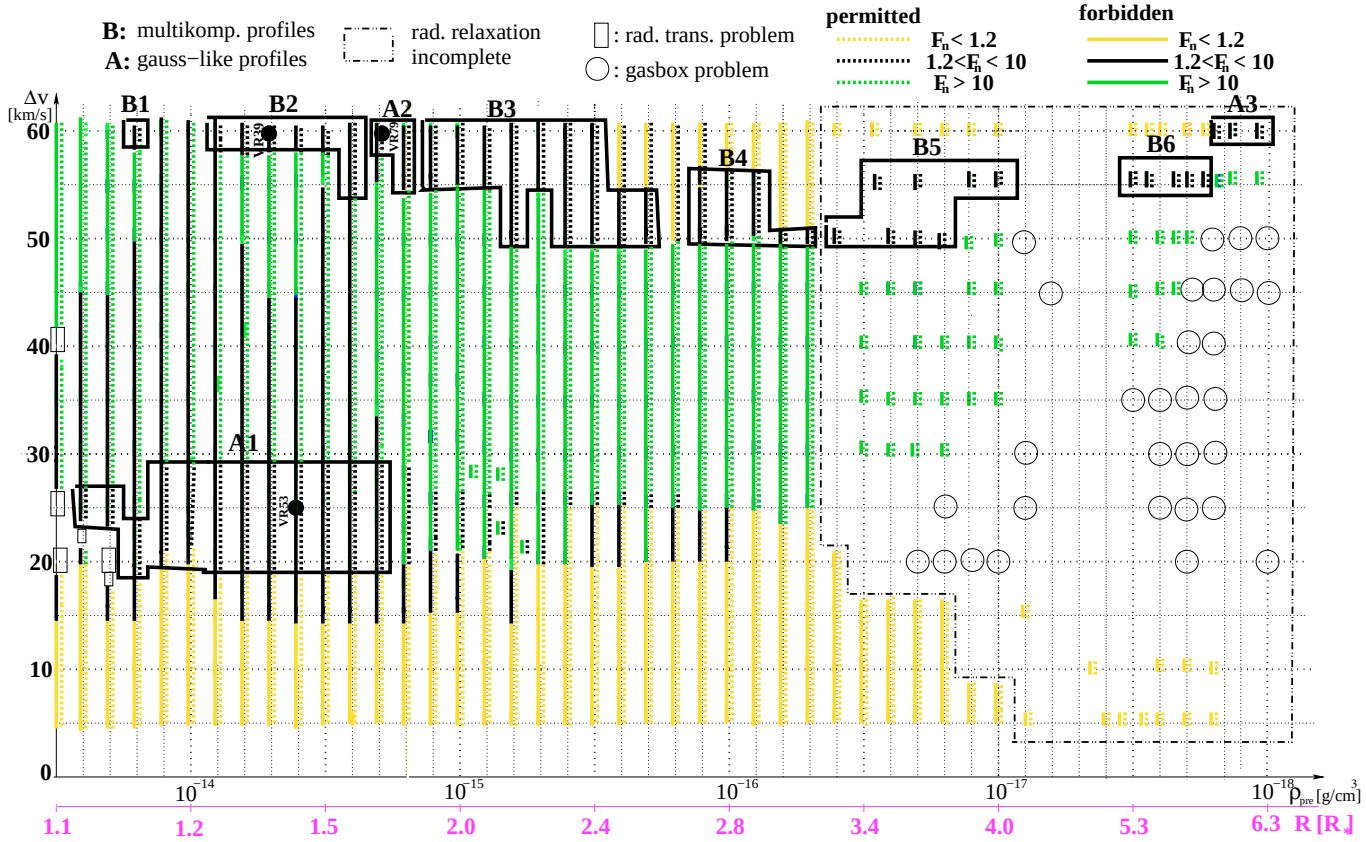

Fig. 6. Similar to Fig. 2 but for models where Δv varies for fixed $\rho_{\rm pre}$, R pairs. Thin rectangles mark parameter values where the radiative transfer calculations failed to converge and circles show parameter values where the gas box calculations failed. A whole domain were the relaxation of the gas-box models towards radiative equilibrium remains incomplete is marked with a dashed-dotted line. Bullets mark models which are depicted in Fig. 5.

5.2. Variation of Δv

The previously presented models have shown that there is only a limited *spatial region* in Mira atmospheres where the appropriate Fe II and [Fe II] emission line fluxes can be formed via shocks. We also found that all models that successfully reproduced observational fluxes had $n_{\rm FeII} \sim 10^5$–$10^{5.5}$ cm^{-3}. However, these models considered a fairly restricted range of shock velocity amplitude Δv, guided by examination of reference hydrodynamical models. Here, our main aim is to vary Δv in order to determine the full unconstrained range of shock velocity amplitude, as well as the pre-shock density, which lead to the formation of the Fe II and [Fe II] emission lines of the observed strength.

For our studies we have calculated about 450 gas-box models for different pre-shock densities $\rho_{\rm pre}$ and shock velocity amplitudes Δv, where now R is related to $\rho_{\rm pre}$ according to the model of Schirrmacher et al. (2002). The results are presented in Fig. 6. We mark with small rectangles domains where our radiative transfer code did not converge and with circles the domains where the gas-box calculations failed. The dashed-dotted box at $\rho_{\rm pre} = 7 \times 10^{-17}$–$1 \times 10^{-18}$ g cm^{-3} in Fig. 6 marks a domain where the relaxation towards radiative equilibrium (RE) in the gas-box models remains incomplete. For such small pre-shock gas densities, the gas cannot radiate away the excess energy dissipated by a shock wave within one period (in particular the molecular cooling is not sufficient to radiate away the energy liberated by the H_2 re-formation) before the next shock wave encounters the gas element. In this case, the pre-shock temperature is higher and the pre-shock density lower than in RE (the pre-shock pressure is considered as fixed here).

5.2.1. Outstanding regions of $\rho_{\rm pre}$, Δv space

In Fig. 6, shocks with low velocity amplitudes $\Delta v < 15$ km s^{-1}, as well as extremely high shock velocity amplitudes $\Delta v \sim 60$ km s^{-1} at $\rho_{\rm pre} = 1 \times 10^{-16}$–$2 \times 10^{-18}$ g cm^{-3} lead to normalised line fluxes which are too small (Fig. 6, light grey lines). There exists an intermediate shock amplitude domain from roughly $\Delta v \sim 30$–45 km s^{-1} and $\rho_{\rm pre} = 3 \times 10^{-15}$–$3 \times 10^{-18}$ g cm^{-3} where all normalised peak fluxes turn out to be too large (Fig. 6, dark grey lines). However, there are two in particular interesting, extended domains: 1. at high shock velocities $\Delta v = 50$–60 km s^{-1} over the whole investigated $\rho_{\rm pre}$-span (here the shocks are capable of dissociating *and* ionising the gas completely, leading to extremely high T_2) and 2. at lower shock velocities $\Delta v = 20$–30 km s^{-1} and $\rho_{\rm pre} \sim 4 \times 10^{-14}$–$3 \times 10^{-15}$ g cm^{-3} where both normalised peak fluxes of the permitted and forbidden Fe II emission lines fit the observed data (Fig. 6, black lines).

A detailed examination of these regions is necessary, because although the fluxes might fit the observed normalised peak line fluxes, the line profiles appear to be very different. For instance, in all of the regions marked with **B** (B1, B2, B3, B4, B5, B5 and B6) we get multicomponent profiles as a result of our radiative transfer calculations (see model VR39 Fig. 5, left panels). These kind of profiles do not bear any similarity to our observed single-peaked, Gauss-like profiles (Richter & Wood 2001).

The only regions with appropriate normalised peak fluxes *and* single line profiles are the ones marked with **A** (A1, A2, A3) in Fig. 6. Although the profiles are not perfectly fitting up to this stage, there is a general trend towards the Gauss-like observed profiles in the named regions, at least for the permitted lines (the forbidden lines tend to have square profiles as expected from unobscured shell emission).

Concerning region A3, it is unlikely that high shock amplitudes of 60 km s^{-1} occur at $R \sim 6\,R_*$ ($\rho_{\rm pre} = 1 \times 10^{-18}$ g cm^{-3}). The hydrodynamical calculation by Schirrmacher et al. (2002) show, that the shock velocity amplitude Δv is large in the innermost $1-4\,R_*$ and decreases as the shock moves further outwards. Another argument against this region is that the emission lines could only be emitted from this region by a shock from the previous pulsation cycle (see explanation given for region B in Sect. 5.1.1).

This leaves us with only two possible regions, which are A1 and A2. There is a markable difference in the shape of the profiles in these regions, namely that the Gauss-like profiles have different width: in region A2 the profiles are wider (Fig. 5, right panels) whereas in region A1 the profiles look similar to the ones in our previous study (Fig. 5, middle panel).

Analyses of the peak line ratio $F_{\rm M38}/F_{\rm 6F}$ ($\sim$1 in our observations) provides an additional constraint. Most of the models in region A1 give a ratio $\sim$1 whereas in region A2 the peak line ratios are always significantly higher at about $F_{\rm M38}/F_{\rm 6F} \sim 3$. This strongly suggests that region A1 is the only region fitting our observed Fe II and [Fe II] emission peak line fluxes.

To summarise, we found a limited parameter range in the $\rho_{\rm pre}, \Delta v$ space which leads to the formation of the observed Fe II and [Fe II] peak line fluxes and line ratios, as well as Gauss-like profiles. We conclude that pre-shock densities of $\rho_{\rm pre} = 3 \times 10^{-15}-4\times10^{-14}$ g cm^{-3} and shock amplitude velocities of $\Delta v = 20-30$ km s^{-1}, are needed to lead to the observed Fe II emission lines. According to the reference model of Schirrmacher et al. (2002) such thermodynamical conditions can exist at a radial distance of of the shock $R = 1.1-1.8\,R_*$.

6. Summary and conclusions

A series of detailed NLTE radiative transfer calculations has been performed on models with periodic shock waves in order to analyse the hydrodynamical conditions which lead to the formation of the observed Fe II and [Fe II] emission lines in M-type Mira variables. Other metal emission lines from Richter & Wood (2001) will be examined in future studies.

Our study reveals that there exists only one region (which we call region A) close to the star's photosphere at $1.2-1.8\,R_*$ where the normalised peak fluxes of both the permitted and the forbidden line fit the observational limits. The pre-shock densities therein fit our reference model reasonably well and the radial position of this region corresponds to the region estimated from the fact that the Fe II and [Fe II] emission lines appear about half a pulsation cycle after the shock emerges from the photosphere.

The variation of region A with velocity amplitude of the shock wave was investigated. Higher (lower) velocities lead to the formation of the observed normalised peak fluxes at lower (higher) pre-shock densities.

We conclude that the ion density of Fe II is the crucial factor for determining the peak fluxes, and deduce that the Fe II emission lines can only originate from the hot post-shock region, where the Fe II density is $n_{\rm FeII} \sim 10^5-10^{5.5}$ cm^{-3}.

We find that the limited parameter range to produce the observed normalised peak fluxes is: pre-shock densities of $\rho_{\rm pre} = 3 \times 10^{-15}-4 \times 10^{-14}$ g cm^{-3} and shock amplitude velocities of $\Delta v = 20-30$ km s^{-1}. According to the hydrodynamical reference model these parameter combinations are given in shocks at $R = 1.1-1.8\,R_*$.

We note that among the optically-visible Miras with $P \sim 300-400$ days, the Fe II and [Fe II] emission lines occur only following a bright maximum: presumably these emission lines are produced by a stronger-than-normal shock. The absence of Fe II and [Fe II] emission lines in most pulsation cycles is most likely due to the shock velocity Δv at $1.1-1.8\,R_*$ being less that the limit of $\sim$20 km s^{-1} which our NLTE radiative transfer models require. This perhaps indicates that current hydrodynamical models such as our reference model, which lead us to predict Fe II and [Fe II] emission lines in every cycle, have shock velocities larger than those in real Miras. In that case, the current hydrodynamical models probably overestimate mass loss rates. Improved modelling of the shock waves and the NLTE radiative transfer in the post-shock region of Miras is required to confirm these suggestions.

Acknowledgements. This work is dedicated to Mt. Stromlo Observatory and the RSAA, which burned down in the devastating bushfires on the 19th of January 2003. Our hearts are with all astronomers who lost their homes and working environment. We would like to thank V. Schirrmacher for his cooperation as well as J. M. Winters and K. S. Jeong for their support. A special thanks goes to D. Mihalas for the fruitful discussions. This work was supported by the German *Deutscher Akademischer Austauschdienst, DAAD* with a HSP III grant, project number D/99/15656 and by the *Deutsche Forschungsgemeinschaft, DFG* project number SE 420/21-1, SE 420/21-2 and Sonderforschungsbereich 555, Komplexe Nichtlineare Prozesse, Teilprojekt B8.

References

Bolick, U., Richter, He., & Sedlmayr, E. 2003, ASP Conf. Ser., Stellar Atmosphere Modeling, in press
Bowen, G. H. 1988, ApJ, 329, 299
Dere, K. P., Landi, E., Mason, H. E., Monsignori Fossi, B. C., & Young, P. R. 1997, A&AS, 125, 149
Feuchtinger, M. U., Dorfi, E. A., & Höfner, S. 1993, A&A, 273, 513
Fleischer, A. J., Gauger, A., & Sedlmayr, E. 1992, A&A, 266, 321
Habing, H. 1996, A&ARv, 7, 97
Höfner, S., & Dorfi, E. 1997, A&A, 319, 648

Huguet, E., Gillet, D., & Lafon, J.-P. J. 1992, A&A, 255, 233
Jeong, K. S. 2000, Ph.D. Thesis, Institut für Astronomie und Astrophysik, TU-Berlin, Germany
Mihalas, D., Kunasz, P. B., & Hummer, D. G. 1975, ApJ, 202, 465
Puls, J. 1991, A&A, 248, 581
Richter, He., & Wood, P. R. 2001, A&A, 369, 1027
Richter, He., Wood, P. R., Woitke, P., Bolick, U., & Sedlmayr, E. 2003, ASP Conf. Ser., Stellar Atmosphere Modeling, in press
Richtmyer, R. D., & Morton, K. W. 1967, Difference Methods for Initial Value Problems (New York: John Wiley & Sons), 2nd edn.
Rybicki, G. B., & Hummer, D. G. 1991, A&A, 245, 171
Schirrmacher, V., Woitke, P., & Sedlmayr, E. 2002, A&A, in preparation
Scholz, M., & Tsuji, T. 1984, A&A, 130, 11
Winters, J. M., Le Bertre, T., Jeong, K. S., Helling, C., & Sedlmayr, E. 2000, A&A, 361, 641
Woitke, P., Krueger, D., & Sedlmayr, E. 1996a, A&A, 311, 927
Woitke, P., Goeres, A., & Sedlmayr, E. 1996b, A&A, 313, 217
Woitke, P., & Sedlmayr, E. 1999, A&A, 347, 617
Wood, P. R. 1979, ApJ, 227, 220